The FASEB Journal article fj.09-136481. Published online October 20, 2009.

The FASEB Journal • Research Communication

TLR2 plays a role in the activation of human resident renal stem/progenitor cells

Fabio Sallustio,[1] Luca De Benedictis,[1] Giuseppe Castellano, Gianluigi Zaza, Antonia Loverre, Vincenzo Costantino, Giuseppe Grandaliano, and Francesco P. Schena[2]

Nephrology, Dialysis and Transplantation Unit, Department of Emergency and Organ Transplantation, University of Bari, Bari, Italy

ABSTRACT **In the past few years, adult renal progenitor/stem cells (ARPCs) have been identified in human kidneys, and particularly in Bowman's capsule and proximal tubules. They may play an important role in the kidney regenerative processes and might prospectively be the ideal cell type for the treatment of both acute and chronic renal injury. In this study, microarray analysis identified 6 gene clusters that discriminated normal human glomerular and tubular ARPCs from renal proximal tubular epithelial cells and mesenchymal stem cells. The top-scored pathway in the ARPC gene expression profile contained growth factor receptors and immune system-related genes, including toll-like receptor 2 (TLR2). Stimulation of TLR2 by ligands that mime inflammatory mediators or damage associated molecular pattern molecules induced secretion of elevated amounts of monocyte chemoattractant protein-1 (MCP-1), IL-6, IL-8, and C3 *via* NF-κB activation. TLR2 stimulation also increased the ARPC proliferation rate, suggesting a role for TLR2 in ARPC activation *via* autocrine signaling. Moreover, TLR2 stimulation improved ARPC differentiation into renal epithelial cells and was responsible of ARPC branching morphogenesis and tubule-like structures formation. For the first time, this study provides a genomic characterization of renal multipotent progenitor cells and shows that TLR2 found on ARPCs might be responsible for their activation in the kidney, orchestrating the activation of crucial signaling networks necessary for renal repair.—Sallustio, F., De Benedictis, L., Castellano, G., Zaza, G., Loverre, A., Costantino, V., Grandaliano, G., Schena, F. P. TLR2 plays a role in the activation of human resident renal stem/progenitor cells. *FASEB J.* 24, 000–000 (2010). www.fasebj.org**

Key Words: renal stem cell · chemokine receptor · complement · MCP-1

KIDNEY, LIKE SKIN AND GUT, has excellent regenerative potential. After injury, the renal tubules can regenerate to preserve functional integrity. Kidney regeneration is sustained by renal proximal tubular epithelial cells (RPTECs), which are known to dedifferentiate, migrate into the areas of damage, and redifferentiate, thereby generating new tubular cells (1, 2). However, the normal repair program of the kidney may not be sufficient to respond to major renal pathologies. Recent studies (3, 4) have indicated that resident adult renal stem/progenitor cells (ARPCs) could participate in this repair process and could find clinical application in the treatment of acute renal failure. A considerable amount of research has focused on the use of stem/progenitor cells to improve regeneration in progressive kidney disease (5, 6). Hematopoietic stem cells (HSCs) have been demonstrated to actively participate in renal regeneration in animal models of acute renal injury (2, 7, 8) but not participate directly in the repair process (9–11).

To date, two apparently distinct populations of multipotent ARPCs have been isolated from human kidney: the first by Bussolati *et al.* (12), from the tubule/interstitium, and the second by Sagrinati *et al.* (13), from the Bowman's capsule. These cells exhibited multipotent differentiation ability by generating tubular epithelial-like, osteogenic-like, adipocyte-like, and neuronal-like cells. When injected into mice with glycerol-induced acute renal injury, these $CD133^+/CD24^+$ ARPCs contributed to tubular regeneration; however, the origin and the characteristics of these ARPCs remain controversial. They may represent a remnant of embryonic stem cells (SCs) in the adult tissue or be populations of bone marrow-derived SCs homed within the kidney and modified by the local microenvironment. Whether resident SCs contribute to the repair of injured kidney under pathophysiological conditions directly or by orchestrating tubular regeneration remains to be determined, but preclinical studies (14) suggest that the administration of exogenous mesenchymal stem cells (MSCs) can ameliorate renal injury and accelerate repair. Recently, Humphreys *et al.* (15) showed that papillary interstitial cells do not directly contribute to renal epithelial cells in a model of unilateral ischemia-reperfusion injury, even if these studies do not rule out a paracrine effect of such cells on the repair process, and it has been demonstrated that

[1] These authors contributed equally to this work.

[2] Correspondence: Nephrology Dialysis and Transplantation Unit, Department of Emergency and Organ Transplantation, University of Bari, Policlinico, Piazza G. Cesare N°11, 70124, Bari, Italy. E-mail: fp.schena@nephro.uniba.it

doi: 10.1096/fj.09-136481

$CD133^+/CD24^+$ renal progenitors can generate podocytes (16).

Here, our aim was to obtain genomic characterization of multipotent $CD133^+/CD24^+$ ARPCs from glomeruli and tubules of adult human kidney. From this characterization emerged a major role of the evolutionarily conserved toll-like receptor 2 (TLR2) as a sensor of tissue damage. Damaged tissue is thought to release molecules called "damage-associated molecular pattern molecules" that activate TLRs and trigger downstream activation of transcription factors that regulate expression of survival genes or proinflammatory cytokines and chemokines (17–19). We show, for the first time, that TLR2 is expressed in ARPCs, suggesting a role for this receptor involved in tissue repair.

MATERIALS AND METHODS

Renal tissue-derived primary cell cultures

Fresh human renal cortical tissue was harvested from patients diagnosed with renal carcinoma. All patients gave signed consent for the use of their tissue for research purposes at the time of radical nephrectomy. Portions of normal-appearing cortex were isolated surgically and examined histologically to exclude presence of carcinoma. Isolation of renal fractions was achieved as reported elsewhere (12, 13) but recovering both glomerular and tubular fractions. Briefly, the samples were reduced to very small fragments using surgical scalpels and forced through a 60-mesh (250-μm) steel sieve to remove the fibrous component. Filtration was facilitated by frequently washing the sieve with Hanks' balanced salt solution (Sigma-Aldrich, St. Louis, MO, USA). The cellular fraction was then passed through a 120-mesh (125-μm) steel sieve to isolate the capsulated glomeruli from the tubular fraction. After several washes, the 2 isolated fractions were cultured separately in EGM-MV medium (Lonza, Valais, Switzerland) supplemented with 20% FBS (Sigma-Aldrich). After 4–5 d, tubular fraction cultures were washed twice with Hanks' buffer to remove nonadherent cells and were checked to exclude the presence of glomeruli. After 1 wk in culture, both the fractions were examined by phase-contrast microscopy. If a sufficient number of adherent capsulated glomeruli released cellular outgrowth, the remainder were removed by washing with Hanks' buffer. In the tubular fraction, cell viability and number were checked before proceeding with magnetic cell separation technology (MACS).

Other cell cultures

MSCs and RPTECs were purchased from Lonza and maintained in the recommended medium, REGM and MSCGM, respectively (Lonza).

CD133 isolation and expansion

The cells of both the glomerular and tubular fractions were detached by trypsin/EDTA digestion and washed twice with ice-cold MACS buffer (PBS pH 7.2 with 0.5% BSA, and 2 mM EDTA). After being passed through a 30-μm filter to remove cell clumps, the cells were counted and incubated for 30 min at 4°C in MACS buffer with the same volume (1 μl/10^5 cells) of FcR blocking reagent and CD133Ab-conjugated magnetic microbeads (Miltenyi Biotec, Bergisch Gladbach, Germany). Cells were then washed, as recommended by the manufacturer, and passed through an MS column (Miltenyi Biotec) under the effect of a magnetic field generated by the Mini MACS Separation Unit (Miltenyi Biotec). The CD133-positive cells retained inside the column were washed 3 times and then eluted once the magnetic field was removed. The eluted cells were resuspended in EGM-MV with 20% FCS and incubated at 37°C with 5.0% CO_2.

Cytofluorimetric determination

ARPCs (10^5/determination) were washed with the manufacturer-recommended buffer before staining. The following antibodies were used: PE-conjugated anti-CD133/2 (293C3), FITC-conjugated anti-CD34, and FITC-conjugated anti-CD45 (all from Miltenyi Biotec); FITC-conjugated anti-CD105 and FITC-conjugated anti-CD24 (all from Serotec, Oxford, UK); and FITC-conjugated anti-CD44 (from Instrumentation Laboratory, Milan, Italy). FITC-conjugated mouse IgG1 (Serotec) was used as an isotype control. In all cytofluorimetric determinations performed using Miltenyi antibodies, nonspecific sites were blocked with the FcR blocking reagent (Miltenyi Biotec). Each determination was performed on 10^5 cells. Cytofluorimetric analysis was performed using a Partec FloMax cytofluorimeter (Partec, Münster, Germany).

Cell immunofluorescence and confocal laser scanning microscopy

The expression of CD133, Pax-2, CD24, CD105, CD44, BMI-1, Oct-4, ACRP30, BSP, Zonula occludens 1 (ZO-1), cytokeratin 19 (CK-19), and von Willebrand factor, Lotus tetragonolobus lectin (Lotus), aminopeptidase A, laminin, and NF-κB nuclear localization were evaluated by indirect immunofluorescence and confocal microscopic analysis on ARPCs fixed in 4% paraformaldehyde. The cells were blocked for 1 h (BSA in PBS, pH 7.4) and then incubated with monoclonal or polyclonal primary antibodies overnight at 4°C or for 2 h at room temperature, respectively. The immune complexes were identified after the incubation of the cells with the specific secondary antibodies for 1 h at room temperature. The cells were washed in PBS after each step, counterstained with To-pro-3 (Molecular Probes, Eugene, OR, USA), mounted in Gel/Mount (Biomeda, Milano, Italy), and sealed with nail varnish. Negative controls were obtained by incubating cells with the blocking solution and then omitting the primary antibody. The stained cells were viewed under the Leica TCS SP2 (Leica, Wetzlar, Germany) confocal laser-scanning microscope using ×40 and ×63 objective lenses. The protein expression of CD133 and CD24 *in vivo* was evaluated by indirect immunofluorescence and confocal microscopy analysis on 7-μm-thick sections from paraffin-embedded human renal biopsies. Immunofluorescence experiments were performed using the following primary antibodies: mouse anti-human CD133/1 mAb (clone AC133; Miltenyi Biotec), mouse anti-human CD133/2 mAb (Miltenyi Biotec), rabbit anti-human Pax-2 pAb (Covance, Princeton, NJ), mouse anti-human CD105 mAb (Abcam, Cambridge, UK), mouse anti-human CD24 mAb (Dako, Glostrup, Denmark), mouse anti-human CD44 mAb (Chemicon, Temecula, CA, USA), mouse anti-human Bmi1 mAb (Upstate Biotechnology, Lake Placid, NY, USA), rabbit anti-human Oct-4 pAb (Abcam), rabbit anti-human adipocyte complement-related protein of 30 kDa (ACRP30) polyclonal Ab (Santa Cruz Biotechnology, Inc., Santa Cruz, CA, USA), mouse anti-human bone sialoprotein mAb (Chemicon), rabbit anti-human ZO-1 polyclonal Ab (Santa Cruz Biotechnology), rabbit anti-human CK-19 mAb (Novus Biologicals, Littleton, CO, USA), mouse anti-human von Willebrand factor mAb (Santa Cruz Biotechnology), rabbit anti-human NF-kB p65 subunit mAb (Santa Cruz Biotechnology), goat

anti-human aminopeptidase A polyclonal Ab (Santa Cruz Biotechnology), rabbit anti-human laminin polyclonal Ab (American Laboratory Products Company, Windham, NH, USA), and mouse anti-human TLR2 mAb (Hycult Biotechnology BV, Uden, NH, USA). The following secondary antibodies were used: Alexa Fluor 555 goat anti-mouse IgG, Alexa Fluor 488 goat anti-rabbit IgG, and Alexa Fluor 488 goat anti-mouse IgG1 (all from Molecular Probes). Staining with FITC-labeled Lotus tetragonolobus lectin (Vector Laboratories, Burlingame, CA, USA) was performed following the manufacturer's instructions. The positive control for NF-kB nuclear translocation analysis consisted of HK2 cells stimulated with CD154 and enhancer for 60 min (Alexis Biochemicals, Lüufelingen, Switzerland).

Cell cloning

Cell cloning was performed by the limiting dilution technique. For each experiment, a minimum of five 96-well culture plates were coated with 20 μg/ml fibronectin. Following trypsin digestion, ARPCs were collected and counted. A volume of cell suspension containing 300 cells was diluted in EGM-MV with 20% FBS such that all wells received 50 μl/well. The plates were then incubated for 60 min at 37°C in 5% CO_2, to allow cells to seed, and wells containing a single-cell were identified. After ~1 wk, the formation of clonal colonies was evaluated. ARPCs clones have been collected from a total of 25 different donors and were then expanded for the subsequent analyses. Each experiment was done on distinct donor-derived clones.

Differentiation

Epithelial and endothelial differentiation experiments were carried out as specified elsewhere (12, 13). The undifferentiated cells were used as negative controls, while HK-2 cells and EA.hy cells were used as positive controls. The extrarenal differentiation experiments were performed using the adipogenic induction/maintenance medium and osteogenic differentiation medium (Lonza), according to the manufacturer's instructions. For adipogenic differentiation, 3 cycles of induction/maintenance were performed. Each cycle consisted of culturing ARPCs in induction medium for 3 d and in maintenance medium for 1–3 d. After 3 complete cycles, the cells were cultured for seven more days in adipogenic maintenance medium, replacing the medium every 2–3 d. For osteogenic differentiation, the cells were grown in osteogenic differentiation medium for 2–3 wk, and the medium was replaced every 3–4 d. The undifferentiated ARPCs were used as negative controls; MSCs were used as positive controls.

Tubular cells were identified by the expression of CK-19 and ZO-1. Endothelial cells were detected by cytofluorimetric analysis for CD105 and through immunostaining for von Willebrand factor. Adipocytes were detected by immunofluorescent staining for ACRP30. Osteoblasts were detected by immunofluorescent staining for sialoprotein.

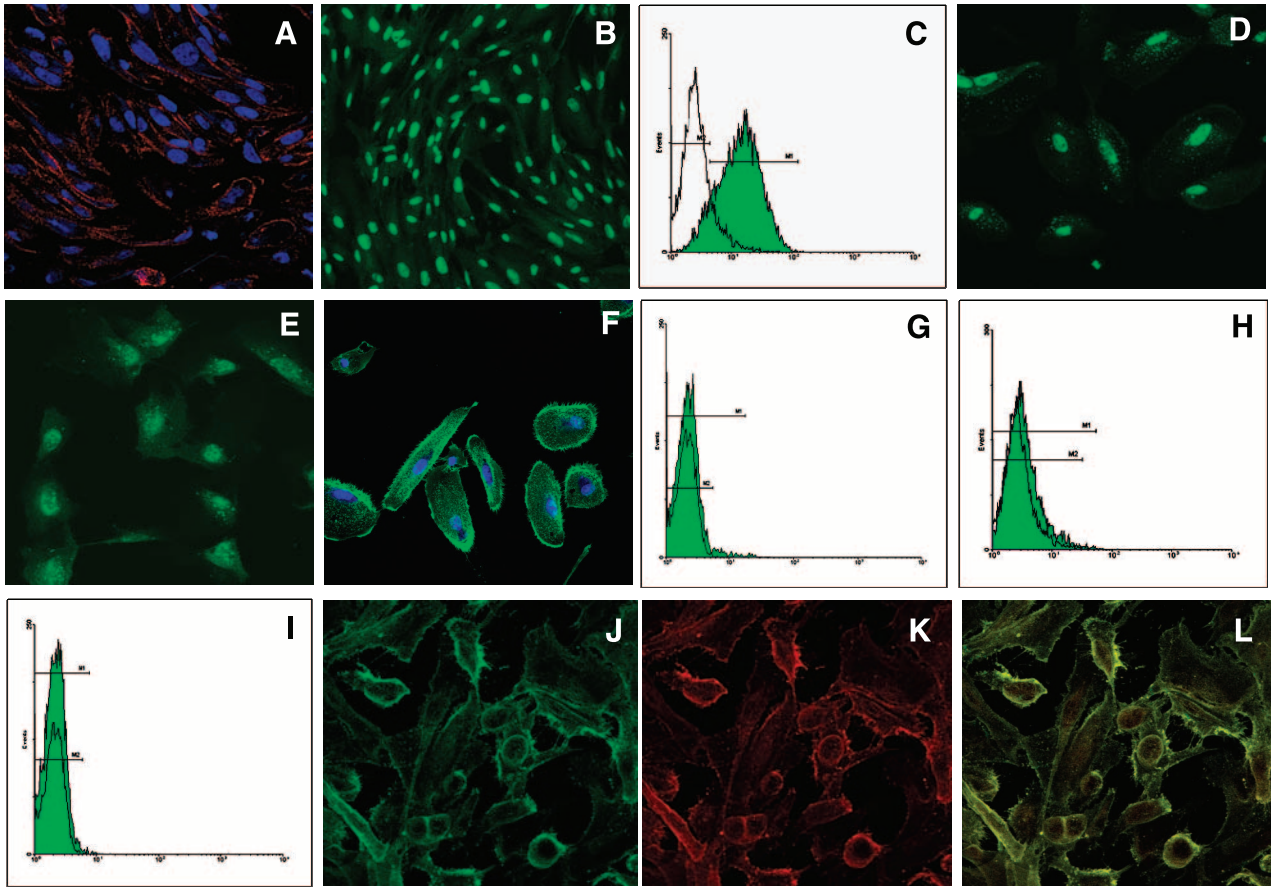

Figure 1. Characterization of isolated ARPCs. *A–I*) Immunofluorescence and cytofluorimetric analysis showed the expression of CD133 (*A*), Pax-2 (*B*), CD24 (*C*), Bmi-I (*D*), Oct-4 (*E*), CD44 (*F*), CD34 (G), CD105 (*H*), and CD45 (*I*). Cell nuclei were visualized using To-pro-3 (blue; *A, F*). *J–L*) Double-label immunofluorescence showing coexpression of CD24 (green) and CD133 (red) by a subset of parietal epithelial cells isolated from tubular fractions. Original view: ×63 (*A, D–F, J–L*); ×40 (*B*).

Microarray hybridization

Total RNA was extracted from a minimum of 10^6 cells/line cultured in quiescence medium (without FBS and growth factors) using the SV Total RNA Isolation Kit (Promega, Madison, WI, USA). Total RNA was quantified by NanoDrop ND-1000 spectrophotometer (Thermo Scientific, Wilmington, DE, USA), and its quality was assessed by 1% agarose gel electrophoresis.

From each cell line, 1.5 μg of total RNA was processed and hybridized to the GeneChip Human Genome U133A oligonucleotide microarray (Affymetrix, Santa Clara, CA, USA). The chip contains 22283 gene probe sets, representing 12357 human genes, plus ~3800 expressed sequence tag clones with unknown function. We used the default settings of Affymetrix Microarray Suite software version 5 (MAS 5.0; Affymetrix) to calculate scaled gene expression values. The data discussed in this publication have been deposited in the National Center for Biotechnology Information's Gene Expression Omnibus (GEO, http://www.ncbi.nlm.nih.gov/geo/) and are accessible through GEO Series Accession Number GSE8611.

Expression data analysis

Expression values for the gene probe sets, scaled to the target intensity of 2500, were log transformed, and ANOVA, distinction calculation (DC), and the Kruskal-Wallis test were used to select probe sets discriminating the 4 cell lines. Gene probe sets were ranked according to their discriminating power (*e.g.*, *P* values in ANOVA and Kruskal-Wallis test contribute to the discriminating component in DC). To further establish whether the selected discriminating gene probe sets were not obtained by chance, we estimated the significance and the false discovery rate using an empirical Bayesian approach based on permutations (n=500) and Storey's q value. R 2.0.1 statistical software was used to perform the above analyses. Principal component analysis (PCA) and 2-dimensional (2-D) hierarchical clustering were performed using Spotfire DecisionSite 9.0 (http://www.spotfire.com).

Real-time PCR

Quantitative real-time PCR reactions were performed using Sybr Green I Nucleic Acid Gel Stain (Molecular Probes), Fluorescein Calibration Dye (Bio-Rad laboratories, Hercules, CA), and Platinum Quantitative PCR SuperMix-UDG (Invitrogen, Carlsbad, CA). For IL-8, WNT7B, DKK3, TLR2, and SMAD3 genes, Quantitect primers (all having annealing temperature of 55°C) were purchased from Qiagen. For PAX8 and HOXA9, the following primer pairs were used (with annealing temperatures of 58°C and 60°C, respectively): PAX-8: forward 5′-ATGGTGGCAGGAAGTGAAT-3′

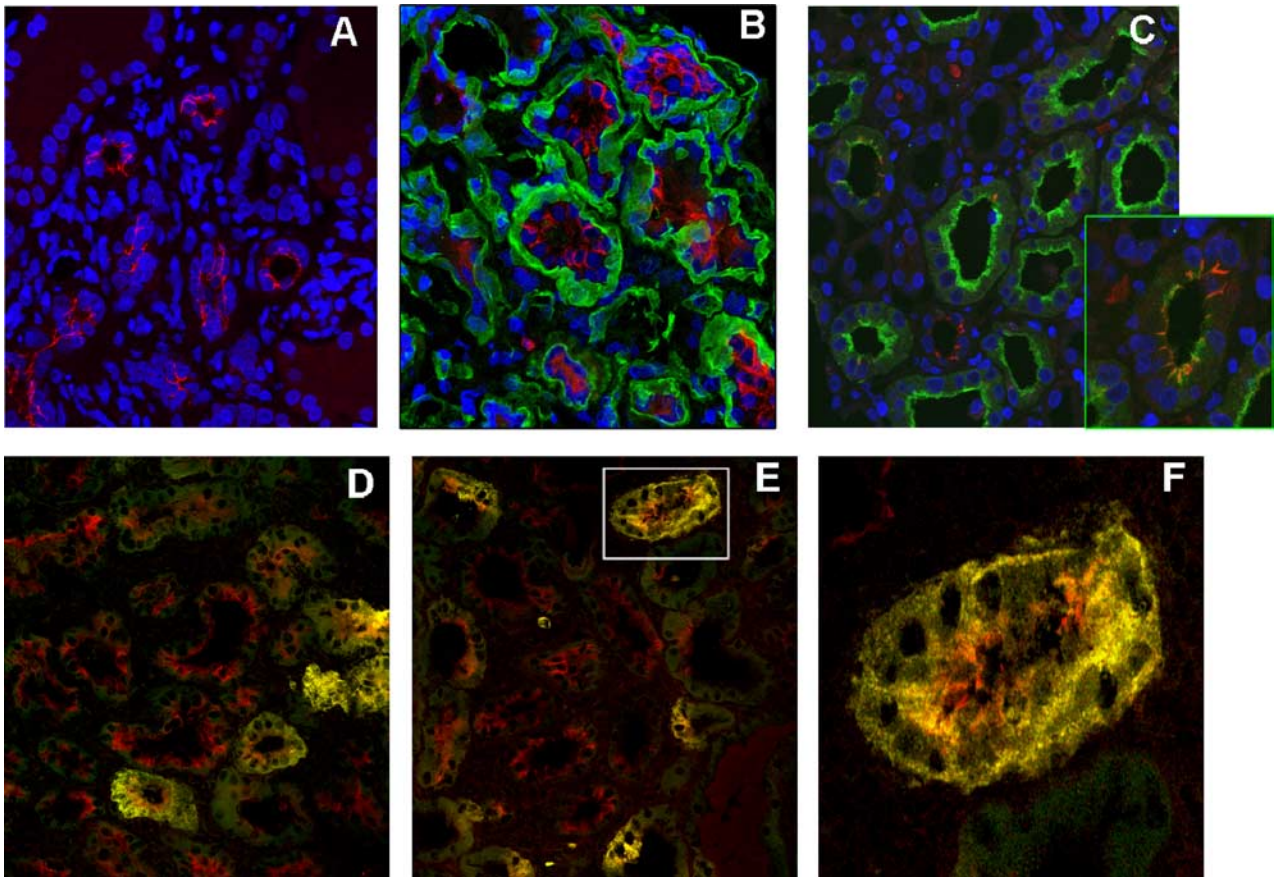

Figure 2. $CD133^+/CD24^+$ progenitor cells localize in tubules. *A*) $CD133^+$ (red) cells were localized in tubules. *B*) Double-label immunofluorescence showing expression of CD133 (red) by cells in tubules (laminin, green) of an adult human kidney. *C*) $CD133^+$ progenitor cells were localized in proximal segment (Lotus, green) of some tubules. Progenitor cells were visible also in distal tubules not stained by Lotus. To-pro-3 counterstains nuclei (blue). *D*, *E*) Double-label immunofluorescence showing expression of CD24 (green) and CD133 (red) by a subset of parietal epithelial cells in some tubules. Merged image demonstrates colocalization of CD24 and CD133 in the cytoplasm and on the membrane of parietal epithelial cells of some tubules. *F*) High-power magnification of a double-label immunofluorescence shows CD24 (green) and apical and lateral membrane CD133 (red) staining in a tubule. Original view ×40 (*A*–*E*); ×7200 (*F*).

and reverse 5′-GGCCTTGATGTGGAACTGTA-3′; HOXA9: forward 5′-CAATAACCCAGCAGCCAACT-3′ and reverse 5′-ATTTTCATCCTGCGGTTCTG-3′. The reaction program included preincubation at 50°C for 3 min; denaturation at 95°C for 5 min; and 40 cycles consisting of denaturation (95°C for 1 min), annealing (annealing temperature for 30 s), and elongation (72°C for 1 min). Melting curves were generated through 100 additional cycles (50°C for 10 s with an increment of 0.5°C/cycle). An iCycler iQ Thermal Cycler (Bio-Rad) was used to perform the reactions.

Pathway analysis

To assess the biological relationships between genes and to obtain maps of cellular pathways, we used Ingenuity software (Ingenuity System, Redwood City, CA, USA; http://www.ingenuity.com), a web-delivered application to discover, visualize, and explore relevant networks of experimental microarray results. Each gene identifier was mapped to genetic networks available in the Ingenuity Pathways Knowledge Base. Genes included in the pathways were not weighted by expression levels, only on biological interactions. The resulting networks were represented in graphic format and adapted for publication.

Detection of secreted cytokines and chemokines

For cytokine/chemokine measurements, 5×10^4 cells were plated in 6-well plates and stimulated with 10 μg/ml lipoteichoic acid (LTA) and 2 μg/ml zymosan. Stimuli were maintained for 24 or 48 h. Subsequently, supernatants were collected after centrifugation at 10,000 *g* for 10 min at 4°C. IL-6, IL-8, and monocyte chemoattractant protein-1 (MCP-1) levels were measured in supernatants using commercial ELISA kits (R&D Systems, Minneapolis, MN, USA), according to the manufacturer's instructions. The concentration of C3 in cell culture supernatants was determined by ELISA: 96-well polystyrene plates were coated with polyclonal rabbit anti-human C3 (Dako, Milan, Italy) diluted 1:500 in carbonate buffer (0.1 M pH 9.6) and incubated for 2 h at 37°C. After blocking with 2% BSA, each diluted supernatant was added in triplicate wells (100 μl/well) and incubated for 2 h. Plates were washed and incubated with horseradish peroxidase-conjugated rabbit anti-human C3c (1:2000 dilution; Dako). The linked enzyme was then developed with ophenylenediamine and incubated at room temperature for 10 min. Optical density was determined at 490 nm. A standard curve was generated using dilutions of a human serum protein standard (Dade Behring, Marburg, Germany). Concentrations of cytokines and chemokines in supernatants were normalized to total cellular protein as determined by Bradford assay.

Transfection with siRNA

siRNA was purchased from Qiagen (Valencia, CA, USA) in 3 formulations. A nonsilencing siRNA sequence, shown by Basic Local Alignment Search Tool (BLAST) search to not share sequence homology with any known human mRNA and tagged with Alexa Fluor 488 (AllStars Negative Control siRNA; Qiagen), was used to determine uptake transfection efficiency. For *in vitro* delivery, siRNA (50 nM) was incubated

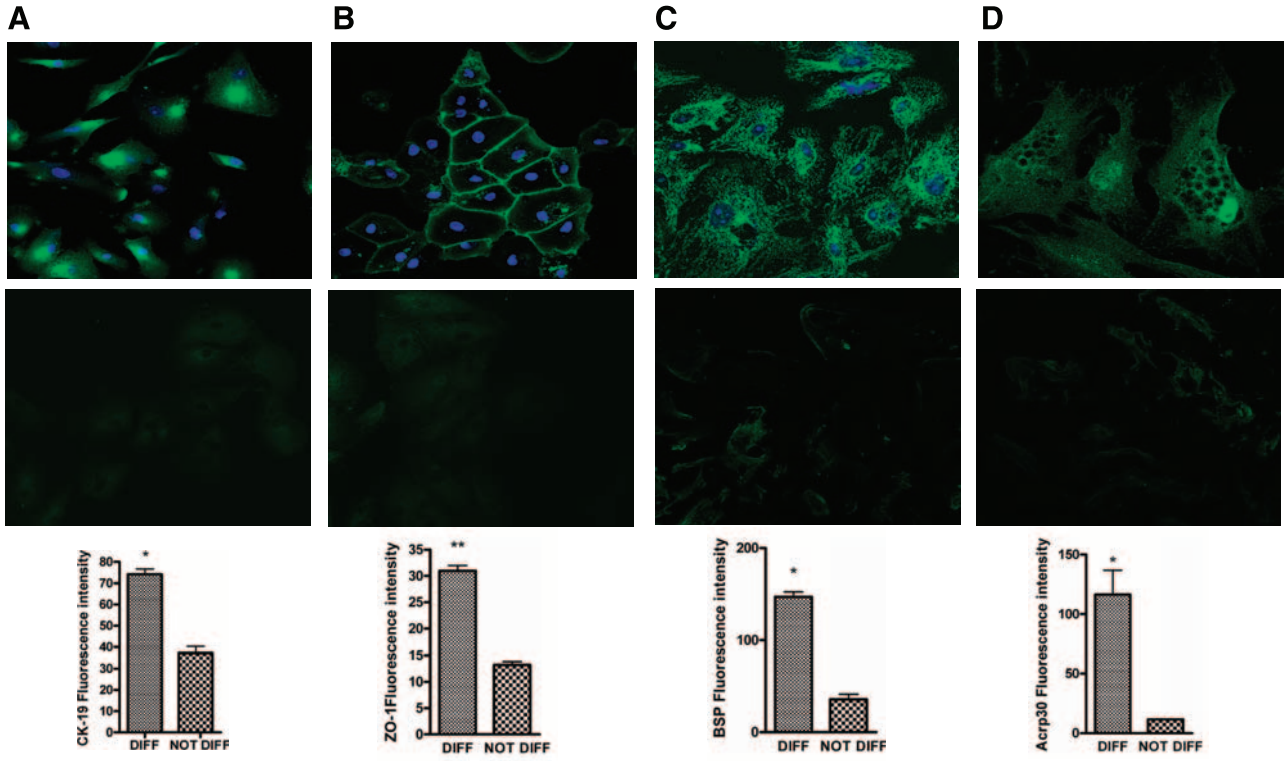

Figure 3. ARPC differentiation. *A*) ARPCs differentiated in renal tubular cells and stained positively for CK-19 (top), negative control (middle), and CK-19 quantization (bottom). *B*) ARPCs differentiated in renal tubular cells stained positively for ZO-1 (top), negative control (middle), and ZO-1 quantization (bottom). *C*) BSP expression observed after osteogenic induction of ARPCs (top), negative control (middle) and BSP quantization (bottom). *D*) ACRP30 was detected after adipogenic differentiation of ARPCs (top), negative control (middle), and ACRP30 quantization (bottom). Original view ×63. $*P < 0.005$, $**P < 0.0007$ *vs.* nondifferentiated cells.

with 6 μl HiPerFect Transfection Reagent (Qiagen) for 10 min at room temperature and added to cells in culture at 80% confluence in 12-well plates. All procedures were performed according to the manufacturer's instructions. Silencing was confirmed by real-time PCR. Functional effects were observed when inhibition of TLR2 expression was ~40% and higher.

Proliferation analysis

Two-day proliferation assays were performed to evaluate the *in vitro* proliferation of ARPCs in response to stimuli. Cells were plated at 5×10^3 cells/well in flat-bottomed 96-well plates (Costar Corning Inc., Life Sciences, Acton, MA, USA) in EGM-MV (Lonza) supplemented with 20% FCS (Sigma-Aldrich). After 24 h, ARPCs were stimulated for 24 h with 10 μg/ml and 20 μg/ml zymosan or 0.5 and 1 μg/ml LTA. Cell proliferation was measured by bromodeoxyuridine (BrdU) incorporation during last 6 h of a 2 d culture by a colorimetric immunoassay, according to the manufacturer's guidelines (Roche Diagnostics, Mannheim, Germany). BrdU absorbance of 1 corresponded to ~6000 cells, whereas BrdU absorbance of 1.4 corresponded to ~35,000 cells. Values were expressed as mean ± SE absorbance at 450 nm − absorbance at 690 nm. All experiments were performed in quadruplicate.

Statistical analyses

We analyzed data with statistical software (GraphPad Prism; GraphPad, San Diego, CA, USA). All data are expressed as means ± SE. We accumulated the data for each condition from ≥3 independent experiments. We evaluated statistical significance with the Student's *t* test for comparisons between 2 mean values. We carried out multiple comparisons between >3 groups with an ANOVA followed by Tukey-Kramer test.

RESULTS

Isolation and characterization of CD133$^+$ renal cell populations

We used magnetic cell sorting to isolate CD133$^+$ cell populations from tubular and glomerular fractions of healthy sections of kidney removed during resection for renal carcinoma from 25 donors. Spindle-shaped cells were plated in EGM-MV with 20% FBS and expanded *in vitro*. The cell lines were homogeneously positive for CD133 antigen by both immunofluorescence (**Fig. 1*A***) and cytofluorimetric (data not shown) analysis. The expression of the renal embryonic transcription factor PAX2 (Fig. 1*B*) and the kidney-specific membrane marker CD24 (Fig. 1*C*) was demonstrated by immunofluorescence and cytofluorimetric analysis, respectively. To exclude the bone marrow as the origin of CD133$^+$ cells, the absence of expression of CD34, CD105, and CD45 membrane proteins was confirmed by cytofluorimetric analysis (Fig. 1*G–I*). Immunofluorescence analysis also confirmed the absence of CD105 expression (data not shown). Finally, we demonstrated that these CD133$^+$ cells expressed the adult SC marker BMI-1 (Fig. 1*D*), the blastocyst SC marker Oct-4 (Fig. 1*E*), and the hyaluronic acid receptor CD44 (Fig. 1*F*). We found

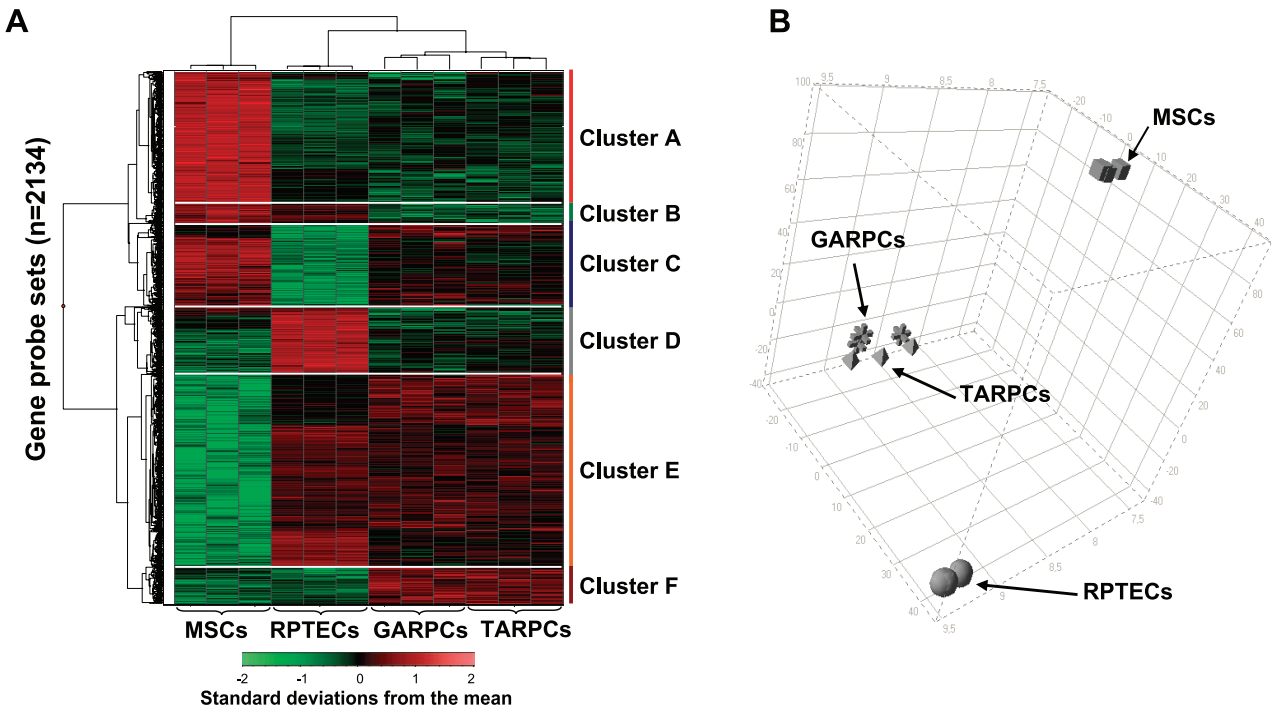

Figure 4. *A*) Two-dimensional hierarchical clustering identified 2134 gene probe sets that discriminated the 4 cell populations ($P<0.0001$; false discovery rate <5%). GARPCs, glomerular adult renal stem/progenitor cells; TARPCs, tubular adult renal stem/progenitor cells. Six gene clusters were identified on the basis of differential gene expression. *B*) Principal component analysis 3-D diagram showing a spatial representation of the differential gene expression. GARPCs and TARPCs are situated close together, having no significant differences in gene expression patterns; RPTECs and MSCs are transcriptionally distant cell populations.

coexpression of CD133 and CD24 markers in a subset of epithelial cells isolated from both glomerular (data not shown) and tubular fractions (Fig. 1*J–L*), showing that we were dealing with renal progenitor cells. We confirmed, *in vivo*, the localization of $CD133^+/CD24^+$ progenitor cells on the tubular epithelium (**Fig. 2**). Progenitor cells were found on both distal and proximal tubular segments (Fig. 2*C*).

Cell cloning and differentiation

Homogenous clonal populations, positive for CD133 and CD24 by cytofluorimetry, were obtained using the limiting dilution technique (data not shown). Three individual clones, of glomerular and tubular origin, were evaluated for their ability to differentiate into renal and nonrenal cell types, and all showed the same differentiation potential. When exposed to tubular cell differentiation medium, the clones expressed CK-19 and ZO-1 in contrast to undifferentiated cells maintained in expansion medium (**Fig. 3*A, B***). Incubation with osteogenic differentiation medium led to the expression of the bone sialoprotein antigen (Fig. 3*C*). After exposure to adipocyte differentiation medium, the clones showed specific positivity for the adipose tissue marker ACRP30, which was not observed in control cells (Fig. 3*D*).

Tubular and glomerular ARPCs have the same gene expression profiles

Cell lines isolated from 3 randomly selected patients were used for large-scale gene expression profiling by oligonucleotide microarray. For each patient, both tubular and glomerular $CD133^+$ populations were included in the study. Expression of the markers CD133, Pax-2, CD24, and Oct-4 in the 6 cell lines was confirmed by immunofluorescence before microarray analysis. To highlight the similarities and the differences with known stem populations and with terminally differentiated renal cells, 3 subcultures of the MSC line and 3 subcultures of the RPTEC line were included in the

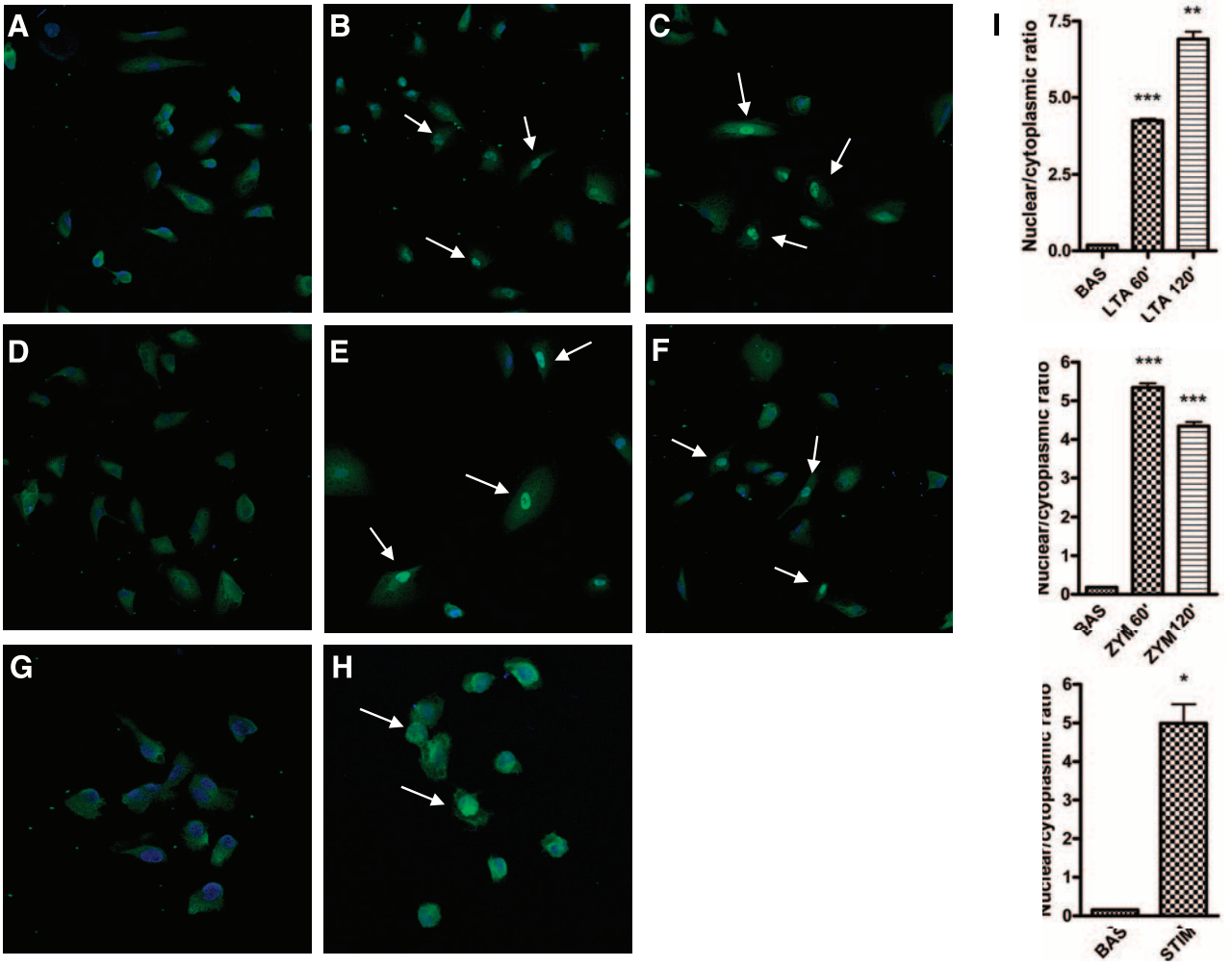

Figure 5. TLR2 stimulation by zymosan and LTA induces NF-κB nuclear translocation in ARPCs. *A–H*) Immunocytochemical analysis of the cellular localization of NF-κB (green, arrows) in ARPCs cultured in the absence (*A, D*) and presence of TLR2 agonists for 60 and 120 min. Cells were treated with 2 μg/ml of LTA (*B, C*) or 10 μg/ml of zymosan (*E, F*) or positive control treatment (*G, H*). *I*) Nuclear/cytoplasmic ratios of NF-κB in ARPCs cultured in the presence of LTA (top) or zymosan (middle) and in controls (bottom); $n = 3$. $^*P < 0.01$, $^{**}P < 0.005$, $^{***}P < 0.0007$ *vs.* unstimulated cells.

analysis. Statistical analysis identified 1742 genes that discriminated ARPCs from RPTEC and MSC ($P<0.0001$, false discovery rate<5%; Supplemental Table 1). Hierarchical clustering (**Fig. 4*A***) and 3-dimensional (3-D) PCA (Fig. 4*B*) demonstrated that the gene expression profiles of glomerular and tubular multipotent ARPCs were not statistically different from one another ($P=0.70$). Thus, from this point onward, we refer to glomerular and tubular multipotent ARPCs by the common designation of multipotent ARPCs.

The 2-D hierarchical clustering identified 149 up-regulated (cluster F) and 71 down-regulated (cluster B) gene probe sets in ARPCs when compared with the MSCs and RPTECs (Fig. 4*A*). Interestingly, 607 gene probe sets (clusters C and D) distinguished the glomerular and tubular ARPCs and MSCs from RPTECs, indicating a possible role for these genes in SC functions. Finally, clusters A (535 gene probe sets) and E (771 gene probe sets) discriminated MSCs from the renal cell lines (Fig. 4*A*; Supplemental Table 2).

Top-scored pathways in the ARPC gene expression profile contain growth factor receptors and immune system-related genes

Pathway analysis was performed on the genes in clusters F and C. The software algorithm identified 12 statistically significant networks related to cluster F (score>1; range, 2–34). The pathway with the highest score included genes involved in proliferative signal transduction (*EGFR*, *IGF1R*, *LIF*, *WNT7A*, and *WNT7B*) and immunoresponse activation (*IL-6*, *IL-8*, and *TLR2*; Supplemental Fig. 1). The genes from both groups were linked by numerous regulatory relationships. The pathway analysis software mapped out 26 differently scored networks in cluster C, 14 of which were statistically significant. These networks included genes involved in various cellular activities: cell commitment (*JAG1*, *NOTCH2*, and *WNT5B*); cell growth (*FGF2*, *FGF6*, *CTGF*, *IGFBP2*, *IGFBP3*, *OSM*, and *RUNX1*); *TGF*-β signaling (*SMAD3* and *INHBA*); extracellular matrix degradation (*MMP19* and *ADAM12*); and cell cycle regulation (*FOSL1*, *JUND*, *CSE1L*, and *CCND1*; Supplemental Table 3).

Validation of microarray analysis

Gene expression data were validated by quantitative real-time PCR. Six differently regulated genes were selected from within the different clusters: *IL-8*, *WNT7B*, *DKK3*, *SMAD3*, *PAX8*, *HOXA9*, and *TLR2*. Each gene was confirmed to possess the previously described differential regulation (all $P < 0.05$; Supplemental Fig. 2).

TLR2 agonists activate the NF-κB pathway in ARPCs

Double-label immunofluorescence experiments confirmed TLR2 expression in ARPCs *in vivo*, as well as in culture (Supplemental Fig. 3). TLR2 activity usually leads to activation of NF-κB, which migrates to the nucleus and binds to DNA, thereby initiating transcription and inducing expression of various genes involved in apoptosis regulation, response to multiple stresses, and the inflammatory response. To assess whether

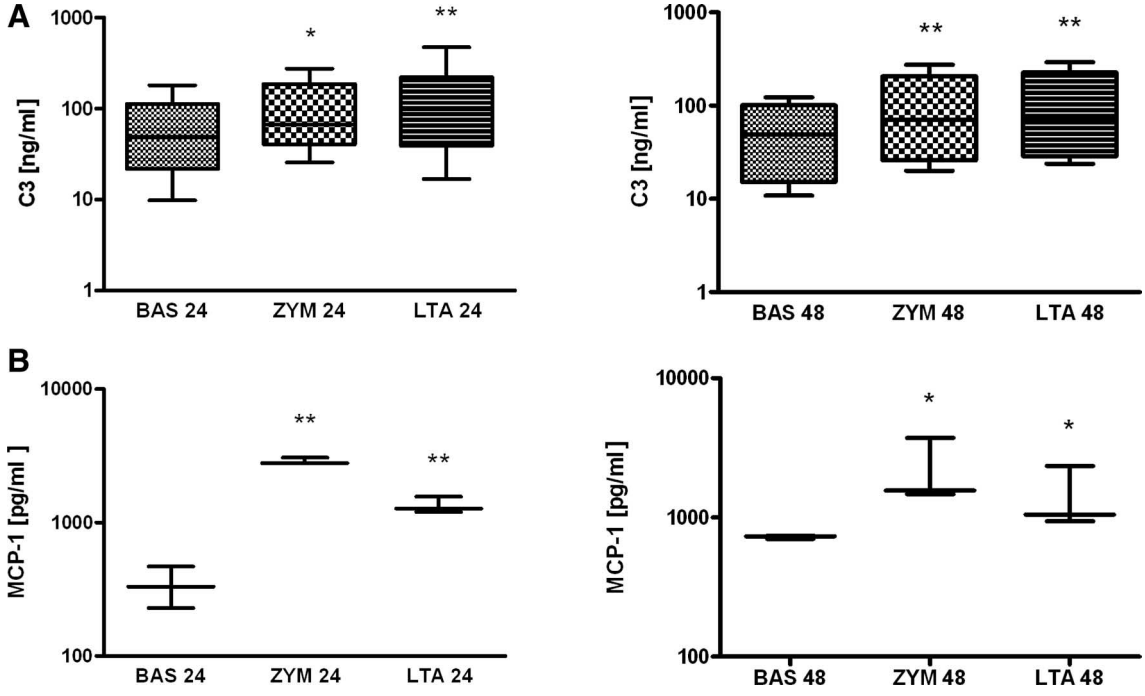

Figure 6. TLR2 stimulation by zymosan and LTA induces C3 and MCP-1 secretion by ARPCs. ARPCs were cultured for 12 and 48 h in the absence or presence of 10 μg/ml zymosan or 2 μg/ml LTA. Levels of C3 (*A*) and MCP-1 (*B*) in the culture supernatants were determined by ELISA. Box plots represent triplicate cultures in 4 experiments; $n = 4$. *$P < 0.05$, **$P < 0.01$ *vs.* unstimulated cells; 1-way ANOVA.

TLR2 stimulation caused NF-κB activation in ARPCs, we analyzed NF-κB p65 localization by immunocytochemical analysis. ARPCs were treated with 2 μg/ml of LTA or 10 μg/ml of zymosan for 60 and 120 min. At baseline, NF-κB was localized mainly within the cytoplasm (**Fig. 5*A***), whereas in the presence of LTA, NF-κB translocated from the cytoplasm to the nucleus at 60 min (Fig. 5*B*) and to a greater extent at 120 min (Fig. 5*C*). In zymosan-stimulated ARPCs, nuclear translocation of NF-κB was observed but was less pronounced than in LTA-treated cells and peaked at 60 min as opposed to 120 min (Fig. 5*E*, *F*). These results confirm the functionality of TLR2 in ARPCs.

TLR2 stimulation induces secretion of C3 and MCP-1

To test whether translocation of NF-κB, induced by TLR2 stimulation, led to the release of proinflammatory factors in ARPCs, we investigated the production and release of 2 NF-κB-dependent factors, C3 and MCP-1, in response to TLR2 activation. Cells were stimulated with 10 μg/ml LTA or 2 μg/ml zymosan for 24 or 48 h, after which culture media were assayed by ELISA. ARPCs showed a significant increase in C3 and MCP-1secretion following stimulation for both 24 and 48 h relative to unstimulated cells (**Fig. 6*A, B***, respectively). Suppression of TLR2 expression, using TLR2-targeted siRNA, yielded a dramatic decrease of chemokines secretion (Supplemental Fig. 4).

TLR2 stimulation induces IL-6 and IL-8 secretion and ARPC proliferation

To investigate proinflammatory cytokines known to participate in the inflammatory response associated with kidney injury, we measured cytokine secretion by ARPCs in response to stimulation by LTA and zymosan. Both stimuli were maintained for 24 or 48 h. As shown in Fig. 6*A*, there were significant increases in IL-6 levels following TLR2 stimulation for 24 ($P<0.01$) or 48 h ($P<0.05$). Stimulation with LTA, but not zymosan, for 24 h also significantly increased IL-8 levels ($P<0.05$). Forty-eight hours of stimulation by both LTA and zymosan provoked significant increases in IL-8 levels ($P<0.05$; **Fig. 7*A***). Suppression of TLR2 expression, using TLR2-targeted siRNA, yielded a dramatic decrease of cytokines secretion (Supplemental Fig. 4).

The relationship between the overexpression of TLR2 and its potential function in ARPCs could indicate a role for TLR2 in modulating the proliferation rate of ARPCs and therefore their capacity for self-renewal. To investigate whether TLR2-dependent signaling influenced the proliferation rate of ARPCs, cells were stimulated for 24 h with 10 and 20 μg/ml zymosan and with 0.5 and 1 μg/ml LT, and cell proliferation was measured by BrdU incorporation. Both zymosan and LTA significantly increased ARPC proliferation ($P<0.05$; Fig. 7*B*), supporting the hypothesis that TLR2 stimulation induces activation of multipotent ARPCs, thereby significantly accelerating their rate of replication.

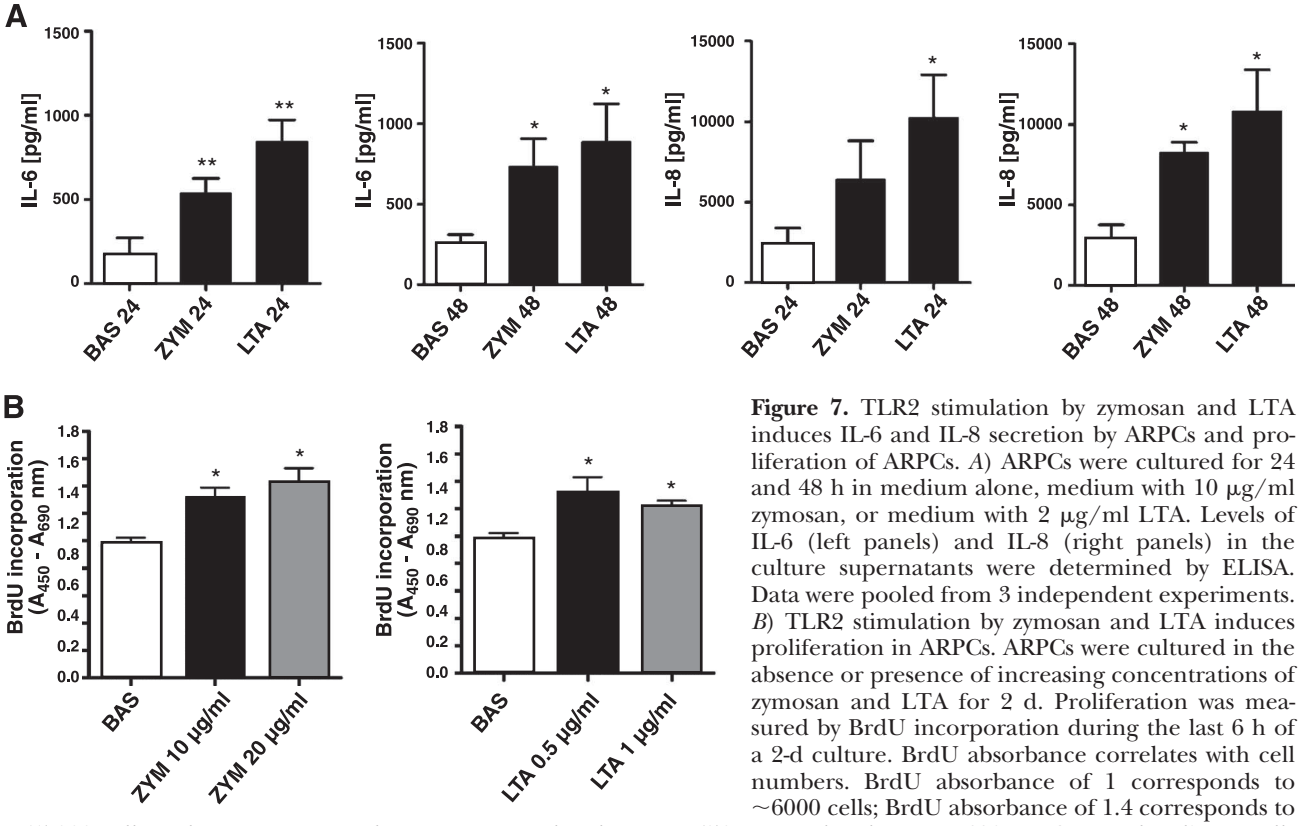

Figure 7. TLR2 stimulation by zymosan and LTA induces IL-6 and IL-8 secretion by ARPCs and proliferation of ARPCs. *A*) ARPCs were cultured for 24 and 48 h in medium alone, medium with 10 μg/ml zymosan, or medium with 2 μg/ml LTA. Levels of IL-6 (left panels) and IL-8 (right panels) in the culture supernatants were determined by ELISA. Data were pooled from 3 independent experiments. *B*) TLR2 stimulation by zymosan and LTA induces proliferation in ARPCs. ARPCs were cultured in the absence or presence of increasing concentrations of zymosan and LTA for 2 d. Proliferation was measured by BrdU incorporation during the last 6 h of a 2-d culture. BrdU absorbance correlates with cell numbers. BrdU absorbance of 1 corresponds to ~6000 cells; BrdU absorbance of 1.4 corresponds to ~35,000 cells. Values are expressed as mean ± SE absorbance at 450 nm − absorbance at 690 nm for quadruplicate wells from 4 separate experiments; $n = 4$. $^*P < 0.05$, $^{**}P < 0.01$ *vs.* unstimulated cells.

TLR2 stimulation improves ARPC differentiation into renal tubular cells

To investigate the role of TLR2 in ARPC differentiation processes, 3 individual ARPC clones, of glomerular and tubular origin, were evaluated for their ability to differentiate into epithelial cell types in the presence or in absence of 10 μg/ml LTA or 2 μg/ml zymosan for 5, 10, 15, and 25 d. When exposed to epithelial cell differentiation medium in the presence of zymosan or LTA, the clones expressed ZO-1 and Lotus after only 10 d of culture, with respect to 25 d needed without TLR2-agonist stimulation. They arranged to form an epithelial carpet, in which epithelial cells are packed tightly together, with almost no intercellular spaces and only a small amount of intercellular substance. In contrast, cells maintained in differentiation medium without TLR2-agonist stimulation were more interspersed, with poor expression of ZO-1 marker and no expression of Lotus (**Fig. 8*A–F***). Enhanced ARPC differentiation was also manifested in an increased percentage of cells expressing the epithelial markers at 25 d (data not shown).

Moreover, when subjected to TLR2 stimuli, ARPCs were able to undergo branching morphogenesis and form tubule-like structures after 10 d of culture (Fig. 8*G–H*), unlike cells without TLR2-agonist stimulation that did not form these structures not even after 25 d of culture. ARPCs forming tubule-like structures expressed laminin, ZO-1, and aminopeptidase A, which are epithelial, basement membranes, and glomeruli and proximal tubular epithelial cell markers, respectively (Fig. 8*I–L*).

DISCUSSION

ARPCs may play an important role in the kidney regenerative processes, and because they display the

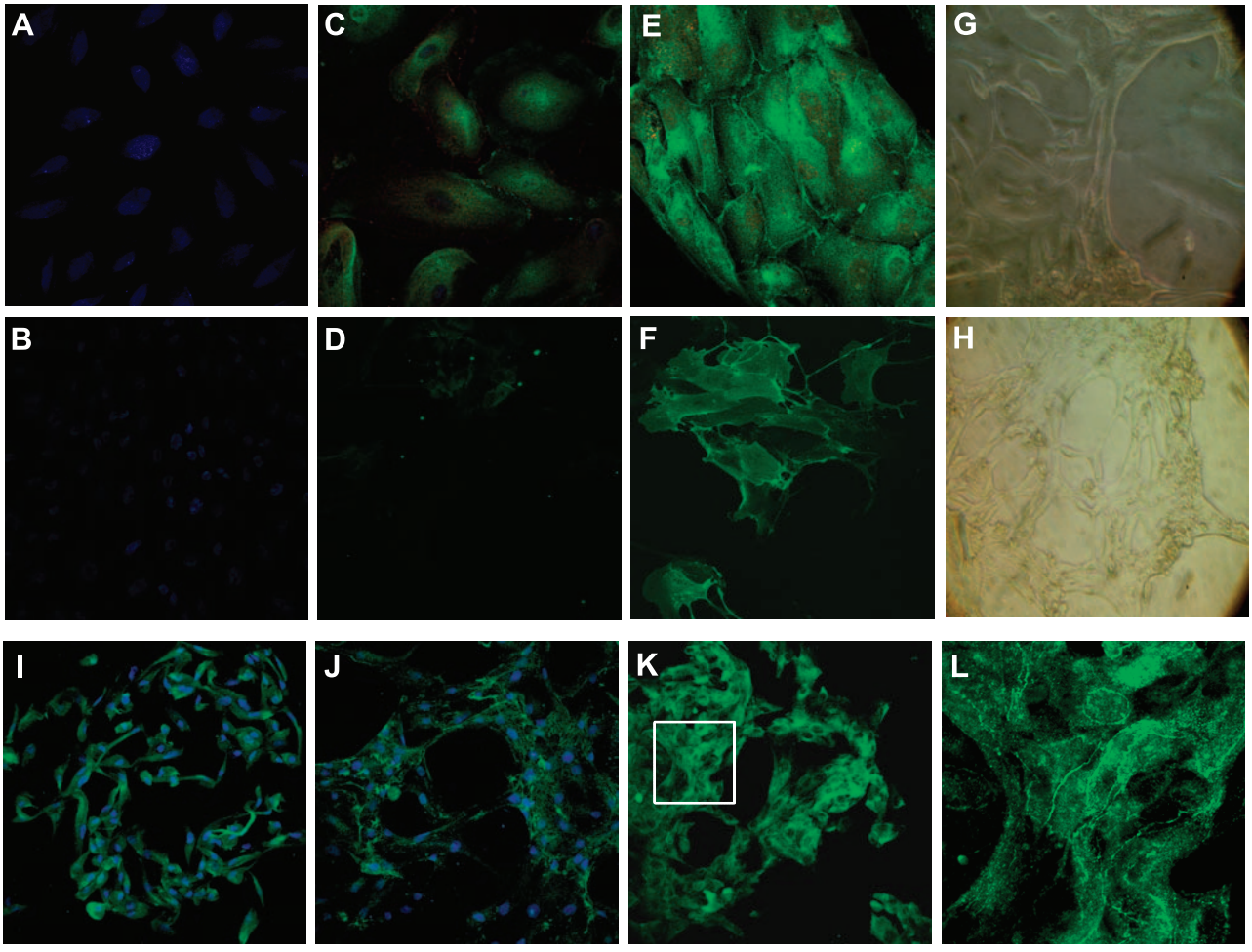

Figure 8. TLR2 stimulation enhances ARPC differentiation into renal epithelial cells. *A, B*) Expression of ZO-1 (*A*) and Lotus (*B*) at d 0. *C, D*) Cells maintained in differentiation medium for 10 d without LTA are interspersed, with poor expression of ZO-1 (*C*) and no expression of Lotus (*D*). *E, F*) In the presence of 10 μg/ml LTA, ARPCs express ZO-1 (*E*) and Lotus (*F*) and arrange to form an epithelial carpet. *G, H*) Representative micrographs showing ARPCs undergoing branching morphogenesis and forming tubule-like structures after 10 d of culture in the presence of LTA. *I*) Expression of aminopeptidase A by ARPCs undergoing epithelial branching morphogenesis following TLR2 stimulation. *J, K*) Expression of laminin (*J*) and ZO-1 (*K*) in tubule-like structures formed by ARPCs in the presence of LTA. *L*) High-power magnification of immunofluorescence showing ZO-1 junctions in tubule-like structures formed by ARPCs. To-pro-3 counterstains nuclei (blue). Original view: ×63 (*A–F*); ×20 (*G*); ×10 in (*H*); ×40 (*I–K*); ×7200 (*L*).

potential to differentiate into multiple renal cell types (3, 4, 14), they could be an ideal tool for treating both acute and chronic renal injury.

We isolated $CD133^+$ cell lines from glomeruli and tubules of human kidneys. The coexpression in these cells of renal progenitor cell markers CD133 and CD24 and of embryonic renal factor PAX2, their clonogenic multipotency, and self-renewal ability demonstrate that these cells are resident ARPCs. We showed that ARPCs were localized also in renal tubules.

Microarray analysis revealed no significant differences in the gene expression patterns of glomerular ARPCs and tubular ARPCs. The 6 cell lines indeed segregated in an interspersed order in the unsupervised hierarchical clustering and the PCA diagram clearly confirmed these data. Therefore, it is conceivable that tubular and glomerular ARPCs represent a genetically homogeneous population.

Interestingly, in the expression analysis, we observed a cluster of genes that discriminated ARPCs from MSCs and normal tubular cells, as well as a cluster of genes that were up-regulated in both SC lines as compared with normal tubular cells. The first cluster included genes involved in proliferative signal transduction (*EGFR*, *IGF1R*, and *LIF*) and immunoresponse activation (*IL-6*, *IL-8*, and *TLR2*). The up-regulation of *EGFR* and *IGF1R* is interesting, since both of these growth factors are known to play important roles during the recovery of the kidney from acute tubular necrosis (20, 21). The second cluster, or the "staminality cluster," included a group of genes whose expression profile was shared by renal and nonrenal stem/progenitor cells. The most significant pathway emerging from this cluster showed the activation of genes involved in cell commitment, cell growth, TGF-β signaling, extracellular matrix degradation, and cell cycle regulation.

The up-regulation of TLR2, a pattern-recognizing receptor involved in innate immune activity, was intriguing because TLR2 could function as a damage sensor in ARPCs (22), which led us to consider a potential role of immune mediators in SC therapy and the treatment of renal failure. The presence of TLR2 in MSCs (23) and adipose-derived stromal cells (24) has already been established, but its presence in ARPCs is novel. However, the role that the receptor plays in SCs, especially in the case of damage, has yet to be established.

Within the kidney, TLR2 is constitutively expressed and plays a crucial role in the induction of acute inflammation and early tubular injury in a reversible model of acute renal injury (25). TLR2 in renal cells contributes to the innate immune response in renal infection, but the recognition of endogenous molecules released from injured cells, such as biglycan or heat shock proteins, may contribute to acute tubular injury and seem to provide adjuvant activity for renal inflammation (26, 27). Recent studies (28) showed that TLR2 initiates a renal inflammatory response but does not play an essential role in the development of progressive renal injury and fibrosis during obstructive nephropathy.

We found that ARPCs secreted MCP-1 and C3, plausibly *via* NF-κB activation (29, 30), in response to TLR2 stimulation. Furthermore, we found that TLR2-agonist stimulation increased the amount of IL-6 and IL-8 cytokines secreted by ARPCs and induced proliferation of ARPCs.

Interestingly, innate immunity and cleavage fragments of C3 play important roles in mobilizing hematopoietic stem/progenitor cells and complement cascade activation products have been found to differentially modulate SC trafficking (31, 32).

Studies have demonstrated that IL-8, a chemoattractant and neutrophil activating factor, can rapidly induce HSC mobilization in primates and in mice (33, 34). In addition, it has been found that MCP-1 activates the migration capacity of rat-derived neural SCs (35), is necessary for homing/recruitment of MSCs (36), and has a dose-dependent migratory effect on human periosteum-derived progenitor cells (37). In addition, MCP-1 may induce the epithelial-to-mesenchymal transition of RPTECs (38, 39). TLR2 stimulation increased the ARPC proliferation rate, suggesting a role for TLR2 in ARPC activation *via* autocrine signaling. Moreover, we showed that TLR2 stimulation improved ARPC differentiation into renal epithelial cells. ARPCs were able to undergo branching morphogenesis and form tubule-like structures exclusively following TLR2 stimulation.

Together, the results from this and our previous studies (14, 40) suggest that ARPCs, following damage sensed by TLR2, could work as directors of the renal regenerative process, controlling the 3 main kidney repair pathways: proliferation and differentiation of resident ARPCs, dedifferentiation and subsequent proliferation of surviving tubular cells (1, 40, 41), and recall of bone marrow SCs (41–42). This study also shows the localization of $CD133^+/CD24^+$ progenitor cells in the tubular epithelium, provides the first genomic characterization of populations of resident multipotent progenitor cells in adult human renal glomeruli and tubules, and shows that TLR2 found on adult ARPCs might be responsible for their activation in repair processes in the kidney. FJ

We thank Michele Battaglia (University of Bari) for harvesting the renal tissue, and Antonio Traficante (Di Venere Hospital, Bari, Italy). We thank Paola Romagnani (University of Florence, Florence, Italy) and Giovanni Camussi (University of Turin, Turin, Italy) for help in laboratory procedures. This study was supported by grants from Regione Puglia (Progetto strategico 2006 PS 144/06) and from the Ministry of University and Research (MIUR; PRIN 2005 069117).

REFERENCES

1. Bonventre, J. V. (2003) Dedifferentiation and proliferation of surviving epithelial cells in acute renal failure. *J. Am. Soc. Nephrol.* **14**(Suppl. 1), 55–61
2. Little, M. H. (2006) Regrow or repair: potential regenerative therapies for the kidney. *J. Am. Soc. Nephrol.* **17,** 2390–2401
3. Sagrinati, C., Ronconi, E., Lazzeri, E., Lasagni, L., and Romagnani, P. (2008) Stem-cell approaches for kidney repair: choosing the right cells. *Trends Mol. Med.* **14,** 277–285
4. Yokoo, T., Kawamura, T., and Kobayashi, E. (2008) Stem cells for kidney repair: useful tool for acute renal failure? *Kidney Int.* **74,** 847–859
5. Chen, J., Park, H. C., Addabbo, F., Ni, J., Pelger, E., Li, H., Plotkin, M., and Goligorsky, M. S. (2008) Kidney-derived mesenchymal stem cells contribute to vasculogenesis, angiogenesis and endothelial repair. *Kidney Int.* **74,** 879–889
6. Plotkin, M. D., and Goligorsky, M. S. (2006) Mesenchymal cells from adult kidney support angiogenesis and differentiate into

multiple interstitial cell types including erythropoietin-producing fibroblasts. *Am. J. Physiol. Renal Physiol.* **291,** F902–912
7. Kale, S., Karihaloo, A., Clark, P. R., Kashgarian, M., Krause, D. S., and Cantley, L. G. (2003) Bone marrow stem cells contribute to repair of the ischemically injured renal tubule. *J. Clin. Invest.* **112,** 42–49
8. Morigi, M., Imberti, B., Zoja, C., Corna, D., Tomasoni, S., Abbate, M., Rottoli, D., Angioletti, S., Benigni, A., Perico, N., Alison, M., and Remuzzi, G. (2004) Mesenchymal stem cells are renotropic, helping to repair the kidney and improve function in acute renal failure. *J. Am. Soc. Nephrol.* **15,** 1794–1804
9. Duffield, J. S., Park, K. M., Hsiao, L. L., Kelley, V. R., Scadden, D. T., Ichimura, T., and Bonventre, J. V. (2005) Restoration of tubular epithelial cells during repair of the postischemic kidney occurs independently of bone marrow-derived stem cells. *J. Clin. Invest.* **115,** 1743–1755
10. Duffield, J. S., and Bonventre, J. V. (2005) Kidney tubular epithelium is restored without replacement with bone marrow-derived cells during repair after ischemic injury. *Kidney Int.* **68,** 1956–1961
11. Nishida, M., Nishida, H., Kawakatsu, H., Shiraishi, I., Fujimoto, S., Gotoh, T., Urata, Y., Ono, T., and Hamaoka, K. (2003) Renal tubular regeneration by bone marrow-derived cells in a girl after bone marrow transplantation. *Am. J. Kidney Dis.* **42,** 10–22
12. Bussolati, B., Bruno, S., Grange, C., Buttiglieri, S., Deregibus, M. C., Cantino, D., and Camussi, G. (2005) Isolation of renal progenitor cells from adult human kidney. *Am. J. Pathol.* **166,** 545–555
13. Sagrinati, C., Netti, G. S., Mazzinghi, B., Lazzeri, E., Liotta, F., Frosali, F., Ronconi, E., Meini, C., Gacci, M., Squecco, R., Carini, M., Gesualdo, L., Francini, F., Maggi, E., Annunziato, F., Lasagni, L., Serio, M., Romagnani, S., and Romagnani, P. (2006) Isolation and characterization of multipotent progenitor cells from the Bowman's capsule of adult human kidneys. *J. Am. Soc. Nephrol.* **17,** 2443–2456
14. Bussolati, B., Tetta, C., and Camussi, G. (2008) Contribution of stem cells to kidney repair. *Am. J. Nephrol.* **28,** 813–822
15. Humphreys, B. D., Valerius, M. T., Kobayashi, A., Mugford, J. W., Soeung, S., Duffield, J. S., McMahon, A. P., and Bonventre, J. V. (2008) Intrinsic epithelial cells repair the kidney after injury. *Cell Stem Cell* **6,** 284–291
16. Ronconi, E., Sagrinati, C., Angelotti, M. L., Lazzeri, E., Mazzinghi, B., Ballerini, L., Parente, E., Becherucci, F., Gacci, M., Carini, M., Maggi, E., Serio, M., Vannelli, G. B., Lasagni, L., Romagnani, S., and Romagnani, P. (2009) Regeneration of glomerular podocytes by human renal progenitors. *J. Am. Soc. Nephrol.* **20,** 322–332
17. Aliprantis, A. O., Yang, R. B., Mark, M. R., Suggett, S., Devaux, B., Radolf, J. D., Klimpel, G. R., Godowski, P., and Zychlinsky, A. (1999) Cell activation and apoptosis by bacterial lipoproteins through toll-like receptor-2. *Science* **285,** 736–749
18. Aliprantis, A. O., Yang, R. B., Weiss, D. S., Godowski, P., and Zychlinsky, A. (2000) The apoptotic signaling pathway activated by Toll-like receptor-2. *EMBO J.* **19,** 3325–3336
19. Matzinger, P. (2002) The danger model: a renewed sense of self. *Science* **296,** 301–305
20. Humes, H. D., Cieslinski, D. A., Coimbra, T. M., Messana, J. M., and Galvao, C. (1989) Epidermal growth factor enhances renal tubule cell regeneration and repair and accelerates the recovery of renal function in postischemic acute renal failure. *J. Clin. Invest.* **84,** 1757–1761
21. Schena, F. P. (1998) Role of growth factors in acute renal failure. *Kidney. Int. Suppl.* **66,** 11–15
22. Anders, H. J., Banas, B., and Schlondorff, D. (2004) Signaling danger: toll-like receptors and their potential roles in kidney disease. *J. Am. Soc. Nephrol.* **15,** 854–867
23. Tomchuck, S. L., Zwezdaryk, K. J., Coffelt, S. B., Waterman, R. S., Danka, E. S., and Scandurro, A. B. (2008) Toll-like receptors on human mesenchymal stem cells drive their migration and immunomodulating responses. *Stem Cells* **26,** 99–107
24. Hwa Cho, H., Bae, Y. C., and Jung, J. S. (2006) Role of toll-like receptors on human adipose-derived stromal cells. *Stem Cells* **24,** 2744–2752
25. Shigeoka, A. A., Holscher, T. D., King, A. J., Hall, F. W., Kiosses, W. B., Tobias, P. S., Mackman, N., and McKay, D. B. (2007) TLR2 is constitutively expressed within the kidney and participates in ischemic renal injury through both MyD88-dependent and -independent pathways. *J. Immunol.* **178,** 6252–6258
26. Anders, H. J., and Schlöndorff, D. (2007) Toll-like receptors: emerging concepts in kidney disease. *Curr. Opin. Nephrol. Hypertens.* **16,** 177–183
27. Lang, A., Benke, D., Eitner, F., Engel, D., Ehrlich, S., Breloer, M., Hamilton-Williams, E., Specht, S., Hoerauf, A., Floege, J., von Bonin, A., and Kurts, C. (2005) Heat shock protein 60 is released in immunemediated glomerulonephritis and aggravates disease: in vivo evidence for an immunologic danger signal. *J. Am. Soc. Nephrol.* **16,** 383–391
28. Leemans, J. C., Butter, L. M., Pulskens, W. P., Teske, G. J., Claessen, N., van der Poll. T., and Florquin, S. (2009) The role of Toll-like receptor 2 in inflammation and fibrosis during progressive renal injury. *PLoS One* **4,** e5704
29. Castellano, G., Cappiello, V., Fiore, N., Pontrelli, P., Gesualdo, L., Schena, F. P., and Montinaro, V. (2005) CD40 ligand increases complement C3 secretion by proximal tubular epithelial cells. *J. Am. Soc. Nephrol.* **16,** 2003–2011
30. Nam, N. H. (2006) Naturally. occurring. NF-kappaB. inhibitors. *Mini Rev. Med. Chem.* **6,** 945–951
31. Ratajczak, J., Reca, R., Kucia, M., Majka, M., Allendorf, D. J., Baran, J. T., Janowska-Wieczorek, A., Wetsel, R. A., Ross, G. D., and Ratajczak, M. Z. (2004) Mobilization studies in mice deficient in either C3 or C3a receptor (C3aR) reveal a novel role for complement in retention of hematopoietic stem/progenitor cells in bone marrow. *Blood* **103,** 2071–2078
32. Reca, R., Cramer, D., Yan, J., Laughlin, M. J., Janowska-Wieczorek, A., Ratajczak, J., and Ratajczak, M. Z. (2007) A novel role of complement in mobilization: immunodeficient mice are poor granulocyte-colony stimulating factor mobilizers because they lack complement-activating immunoglobulins. *Stem Cells* **25,** 3093–3100
33. Fibbe, W. E., Pruijt, J. F., van Kooyk, Y., Figdor, C. G., Opdenakker, G., and Willemze, R. (2000) The role of metalloproteinases and adhesion molecules in interleukin-8-induced stem-cell mobilization. *Semin. Hematol.* **37,** 19–24
34. Laterveer, L., Lindley, I. J., Hamilton, M. S., Willemze, R., and Fibbe, W. E. (1995) Interleukin-8 induces rapid mobilization of hematopoietic stem cells with radioprotective capacity and long-term myelolymphoid repopulating ability. *Blood* **85,** 2269–2275
35. Widera, D., Holtkamp, W., Entschladen, F., Niggemann, B., Zanker, K., Kaltschmidt, B., and Kaltschmidt, C. (2004) MCP-1 induces migration of adult neural stem cells. *Eur. J. Cell Biol.* **83,** 381–387
36. Belema-Bedada, F., Uchida, S., Martire, A., Kostin, S., and Braun, T. (2008) Efficient homing of multipotent adult mesenchymal stem cells depends on FROUNT-mediated clustering of CCR2. *Cell Stem Cell* **2,** 566–575
37. Stich, S., Loch, A., Leinhase, I., Neumann, K., Kaps, C., Sittinger, M., and Ringe, J. (2008) Human periosteum-derived progenitor cells express distinct chemokine receptors and migrate upon stimulation with CCL2, CCL25, CXCL8, CXCL12, and CXCL13. *Eur. J. Cell Biol.* **87,** 365–376
38. Li, M., Hering-Smith, K. S., Simon, E. E., and Batuman, V. (2008) Myeloma light chains induce epithelial-mesenchymal transition in human renal proximal tubule epithelial cells. *Nephrol. Dial. Transplant.* **23,** 860–870
39. Wynn, T. A. (2008) Cellular and molecular mechanisms of fibrosis. *J. Pathol.* **214,** 199–210
40. Loverre, A., Capobianco, C., Ditonno, P., Battaglia, M., Grandaliano, G., and Schena, F. P. (2008) Increase of proliferating renal progenitor cells in acute tubular necrosis underlying delayed graft function. *Transplantation* **85,** 1112–1119
41. Humphreys, B. D., Duffield, J. S., and Bonventre, J. V. (2006) Renal stem cells in recovery from acute kidney injury. *Minerva Urol. Nefrol.* **58,** 329–337
42. Gupta, S., Verfaillie, C., Chmielewski, D., Kim, Y., and Rosenberg, M. E. (2002) A role for extrarenal cells in the regeneration following acute renal failure. *Kidney Int.* **62,** 1285–1290

Received for publication May 20, 2009.
Accepted for publication September 24, 2009.